Effect of magnesia-to-phosphate ratio on the passivation of mild steel in magnesium potassium phosphate cement

Wang, Danqian; Yue, Yanfei; Mi, Tangwei; Yang, Siyu; McCague, Colum; Qian, Jueshi

DOI:
10.1016/j.corsci.2020.108848

Publication date:
2020

Effect of magnesia-to-phosphate ratio on the passivation of mild steel in magnesium potassium phosphate cement

Danqian Wang[1], Yanfei Yue[2*], Tangwei Mi[1], Siyu Yang[1], Colum McCague[3,1], Jueshi Qian[2], Yun Bai[1**]

1 Advanced & Innovative Materials (AIM) Group, Department of Civil, Environmental and Geomatic Engineering, University College London, London, UK, WC1E 6BT

2 College of Materials Science and Engineering, Chongqing University, Chongqing 400045, PR China

3 Mineral Products Association, Gillingham House, 38-44 Gillingham Street, London, UK, SW1V 1HU

Corresponding author's email address: * yanfei.yue@cqu.edu.cn; ** yun.bai@ucl.ac.uk;

Danqian Wang: danqian.wang.16@ucl.ac.uk

Tangwei Mi: tangwei.mi.15@ucl.ac.uk

Siyu Yang: siyu.yang.14@ucl.ac.uk

Colum McCague: Colum.McCague@mineralproducts.org

Jueshi Qian: qianjueshi@163.com

Abstract

The low pH of magnesium potassium phosphate (MKPC) has raised concerns over its capability to protect reinforcing steel. The passivation of mild steel in MKPC pore solutions was investigated in this study via electrochemical measurements, XPS and Raman spectroscopy. Results show that the passivity of mild steel in MKPC was comparable or even better than that in Portland cement. Although the passivity was dominated by the pH of MKPC,

it also increases with increasing magnesium-to-phosphate (M/P) ratios. The formation of iron phosphate in the low pH MKPC (such as M/P 7) also made additional contributions to the passivity of steel.

Key words: Mild steel; Passivity; Phosphate; M/P ratio; XPS; Raman spectroscopy

1 Introduction

The reinforcing mild steel embedded in Portland cement concrete may remain chemically stable due to the spontaneous formation of a protective passive film on the surface of mild steel. The passivation process involves electrochemical redox reactions that occurs on the steel surface through its interaction with the alkaline pore solution of concrete [1]. The passive film formed on the mild steel in Portland cement concrete is typically composed of an outer layer of Fe(III) oxides and an inner layer of Fe(II) oxides which are thermodynamically stable in the alkaline condition of Portland cement concrete [2, 3]. However, the exact composition, structure and protective capability of the passive film to be formed, which essentially determines the corrosion resistance of steel, is significantly influenced by the pore solution chemistry of concrete [4, 5]. Among various factors, there is wide agreement that only at a pH value of above c.a. 10.5, a protective passive film can be formed on the surface of steel [6, 7]. As long as this high pH environment is maintained, the passive film is chemically stable and, hence, can provide a good protection to steel. On the contrary, the low pH, such as a pH below 10.5, could result in an increased dissolution of Fe as well as the increased precipitation of FeOOH, leading to the formation of a more porous and less protective passive film on the surface of steel [8]. Furthermore, the presence of some inorganic species, such as phosphate ions, could also be able to improve the corrosion resistance of mild steel in corrosive conditions [9-11]. The corrosion inhibition mechanism of phosphate ions for mild steel can be different in different conditions, which is possibly dependent on the pH condition [9] and the concentration of phosphate ions [10, 11]. For example, Mohagheghi and Arefinia [9] reported

that corrosion was inhibited by the adsorption of phosphate ions in a mildly alkaline solution while precipitation of iron phosphates occurred in a highly alkaline solution. In another study, Dhouibi et al. [11] claimed that phosphate ions of high concentration can act as an anodic inhibitor, while low concentration of phosphate ions act as a cathodic inhibitor in calcium hydroxide solution. Moreover, the inhibition mechanism of phosphate ions in the chloride-contaminated alkaline solution was also found to be related to the formation of insoluble iron phosphate complexes on the steel surface [9, 12] or the formation of compact iron oxides on the steel surface [11].

Magnesium phosphate cement (MPC) is attracting interest as a rapid repair material for concrete structures, primarily due to its fast setting, high early strength and good bond to the existing concrete [13]. Unlike conventional Portland cement (PC), which reacts directly with water to form a cohesive and strong monolith, MPC reacts by means of an acid-base reaction between magnesium oxide (MgO) and a soluble acid phosphate. Although both ammonium and potassium phosphate can be used as a phosphate source to formulate MPC, potassium dihydrogen phosphate, KH_2PO_4 (KDP), is often preferred. This is because, unlike ammonium phosphate, KDP does not liberate ammonia gas during hydration and is, therefore, more suitable for practical applications due to the reduced health and safety concerns [14]. This acid-base reaction between MgO and KDP (as exemplified in Equation 1 below) can also yield a hard and dense cementitious material with very low solubility, making it a possible alternative to PC for construction applications.

$$MgO + KH_2PO_4 + 5H_2O \rightarrow MgKPO_4.6H_2O \qquad \text{Eq.1}$$

According to Eq. 1, in theory, a stoichiometric 1:1 molar ratio of MgO to KDP (M/P) should be adopted to formulate magnesium potassium phosphate cement (MKPC). However, in practice, a higher M/P is often needed in order to formulate a stable MKPC matrix. Although some researchers reported an increase in compressive strength with an increase of M/P, there is now wide agreement that the properties of MKPC are not a monotonic function of M/P. Instead, for a given water/cement ratio (W/C), an optimal M/P is determined for developing the best

mechanical and durability properties. For example, it has been reported that the M/P ratio of 6 was found to be the optimal M/P for achieving the highest strength and lowest permeability at a W/C of 0.20 [15, 16]. To explain this phenomenon, a three-limit theory has been developed and proposed for the mix design of MKPC based materials [17]. Additionally, it has been considered that by using a M/P higher than that based on theory, an excess of MgO is available for reaction. As a result, most of the phosphate can be consumed in the reaction, which not only can reduce the leaching of phosphate and therefore improve the integrity of the hardened MKPC, but also can improve the volume stability of the hardened MKPC [18]. On the other hand, due to the very high reaction rate of MgO and KH_2PO_4, MKPC paste hardens within several minutes, causing some operational issues. In order to slow down the early hydration reaction, dead-burnt MgO is usually used. Additionally, retarders such as boric acid or borax are also used to modulate the setting time [19, 20] which is mainly attributed to the precipitation of magnesium borate compounds around the basic magnesia grains, delaying the reaction with acidic phosphate solution [20].

Furthermore, as illustrated in Eq. 1, when MgO and KH_2PO_4 are mixed with water, a neutralisation reaction occurs between MgO and phosphates, with the former providing alkalinity and the latter acidity. Therefore, unlike Portland cement, which can generate a high internal pH (usually around 13), MKPC paste normally produces a much lower pH environment, in particular, during the early stages of hydration. This can be clearly seen in Fig. 1, in which the pH values of the MKPC reported in the literature have been summarized and plotted. It is evident that the initial pH is usually lower than 7 since at the beginning of the reaction the acidic KH_2PO_4 is believed to dominate the pH of the pore solution [21]. With ongoing hydration, the pH of MKPC starts to increase, reaching the weakly alkaline range. Furthermore, it can be deduced from Fig. 1 that the pH of MKPC generally increases with increasing M/P ratio. For example, the measured pH value at M/P 10 is around 8 at one day hydration [22, 23], at M/P 13 around 9.2 at one day [24], and at M/P 20 around 11 at 10 h [25]. However, most of the reported pH values in Fig. 1 are lower than 10.5. This ‘low’ pH may raise concerns over the

wider application of MKPC in reinforced concrete structures since it may not favour the formation of the protective passive film on the surface of reinforcing steel in the first instance, making the steel less resistant to corrosion.

Nevertheless, some researchers have claimed, albeit based on some limited studies, that MKPC provides the reinforcing steel with comparable protection against chloride-induced corrosion when compared with PC [26, 27]. This finding is, somehow, beyond normal expectations, because it is questionable whether a proper passive film can be formed initially under such a low pH environment of MKPC. However, Zhang et al. [27] has ascribed the good corrosion resistance of reinforcing steel to the good corrosion inhibition provided by the phosphate in MKPC. This hypothesis has been further corroborated by a report that a protective passive layer consisting of iron and phosphate formed when a slurry of acid phosphate with base minerals and metal oxides was sprayed on the steel surface [28]. Although the exact mechanism responsible for this improved corrosion resistance is yet to be understood, it has been hypothesised that the phosphate ions in MKPC may have played an important role. This hypothesis has been deduced from the fact that the phosphate ion, which is a good inhibitor, can promote the formation of some insoluble ferrous phosphate compounds on the steel surface, inhibiting further corrosion processes when exposed to chloride attacks. Therefore, even though the pH of MKPC would not favour the formation of passive film, it has been considered that the phosphate ions present in the MKPC pore solution could potentially benefit the corrosion resistance of rebar. While this hypothesis seems plausible, the passivation behaviour and the passivation mechanism of the steel in MKPC are still largely unknown. In particular, the influence of the M/P ratio, an important parameter for designing MKPC, on the passivation behaviour and underlying passivation mechanism is yet to be understood, even though a good understanding on this is important for designing and predicting the durability and service life of reinforced MKPC concretes in real applications.

In this paper, a systematic study was carried out to investigate the passivation behaviour of reinforcing mild steel immersed in MKPC pore solutions. MKPCs with different M/P ratios were

purposely formulated to generate a range of pH and phosphate environments with an attempt to clearly identify the effects of pH and phosphate on the passivation of the reinforcing steel. The passivation behaviour of the mild steel in MKPC pore solutions was assessed using a suite of electrochemical methods which included linear polarization resistance (LPR), electrochemical impedance spectroscopy (EIS) and potentiodynamic polarization. The chemical composition of the passive film formed in the MKPC pore solution was then characterised by X-ray Photoelectron Spectroscopy (XPS) and Raman spectroscopy. Based on the data obtained, a possible passivation mechanism of the mild steel in MKPC is then proposed and discussed in this paper.

2 Experimental

2.1 Materials

To formulate the MKPC pastes, an industry grade dead burnt magnesia (DBM) was supplied by Changyi New Materials Ltd. from Guangzhou, China and a reagent grade potassium dihydrogen phosphate (KH_2PO_4, KDP) by Prayphos^{TM} with a purity of 98%. Borax ($Na_2B_4O_7 \cdot 10H_2O$) sourced from Sigma-Aldrich with a purity of more than 99.5% was employed as a retarder. A CEM I Portland cement (PC) conforming to BS EN 197-1:2011 supplied by Quinn Cement (Ireland) was used to manufacture a control cement paste. The chemical composition of the PC is shown in Table 1. Mild steel of Φ 16 mm was chosen as the reinforcing steel in this study as it is the most widely used reinforcing material in reinforced concrete. The chemical composition of the mild steel is presented in Table 2.

2.2 Mix design

MKPC pastes with different M/P ratios, namely 7, 12 and 17, were formulated. These M/P ratios were determined based on typical values reported in the literature [18, 24]. Based on some initial trials, the water-to-cement ratio (W/C) was fixed at 0.22 for all the MKPC mixes which has shown to be able to produce MKPC mixes with sufficient fluidity for casting and

specimen preparation. Borax added at 15%wt MgO allowed acceptable working times for the MKPC pastes. The final MKPC mix formulations thus obtained as well as the batch weights of the constituent materials adopted in this study are presented in Table 3. In addition, a PC paste with W/C of 0.45 was employed as a control in the current study in order to compare the performance of mild steel in PC with those in the MKPC systems. The W/C of 0.45 was determined through trials on the basis of achieving a similar paste fluidity as those of the MKPC pastes.

2.3 Manufacture of the paste specimens

Constituent powders were dry-mixed for one minute and then further mixed for another three minutes after adding water in a vertical-axis planetary mixer. The resulting paste was then used to cast the specimens for the pore solution extraction. The specimens were cast in cylindrical polyethylene moulds (90 mm x Φ 35 mm), cured in the moulds and stored in a room at a constant temperature of 20°C for 24 hours first before being demoulded. This particular curing regime was adopted in the current study due to the following considerations. Firstly, due to the fact that the hydration of MKPC is affected by temperature (similar to conventional PC), all the samples in this study were therefore cured at a constant temperature of 20°C in order to eliminate this effect. This would ensure that all the properties could be compared on a like-for-like basis. In addition, based on some initial trials, it was found that there is a need to cure MKPC pastes for 24 hours at 20°C to ensure that pastes with different M/P ratios can all develop the minimum strength needed for demoulding without causing any damage [18, 29, 30]. On the other hand, preliminary trials have also indicated that 24-hour is the minimum time needed for the MKPC pastes to develop a relatively stable pore solution for the subsequent passivation study [23, 24, 31].

2.4 Pore solution extraction

The hardened pastes were taken out from the moulds for the pore solution extraction after being cured for 24 hours. The pore solutions of different mixes were obtained by following the

method first described by Longuet [32] and Barneyback and Diamond [33]. A schematic illustration of the pore solution expression apparatus is shown in Fig. 2. A paste specimen was directly placed in the cavity under the piston. The pore solution extraction apparatus was then subjected to a compressive pressure of 400 MPa using a Universal Tester machine. This level of pressure was maintained for 15 minutes while the pore solution was collected through a pipe connected to the cavity of the extraction apparatus. From each cylinder specimen, around 10 ml pore solution could be collected and at least three specimens were expressed which allowed a sufficient amount of pore solution to be collected for the subsequent pH, ion chromatograph (IC) and passivation tests as described below.

2.5 Test methods

In this study, a range of test methods have been used not only to investigate the passivation behaviour of mild steel in MKPC, but also to characterise MKPC pore solutions. Additionally, some techniques have also been used to characterise the chemical composition of the passive film formed. The details of each test method are given below.

2.5.1 Characterisation of the chemical composition and pH of the pore solution

The concentration of phosphate ions in different MKPC mixes was determined by measuring the phosphate ion in the extracted pore solution. The pore solution was collected from the pore solution expression apparatus using a syringe and filtered through a 0.45 μm filter paper. The filtered pore solution of different MKPC mixes was then diluted at various dilution factors depending on the concentration of phosphate ions in order to meet the requirements of the ion concentration limit specified in the ion chromatograph (IC) test. The diluted solution was subsequently analysed by a Dionex ICS 900 ion chromatograph analyser to determine the concentration of phosphate ions in the pore solution.

The pH of the extracted MKPC pore solutions was determined by a Thermo Scientific Orion 8165BNWP-ROSS Sure-Flow pH electrode. The measurement was taken at intervals of one

second up to approximately 3 minutes until a stabilised pH value was reached, which was then reported as the pH value of the extracted pore solution.

2.5.2 Passivation of mild steel

Thermodynamic and kinetic information relating to the passivation of mild steel was obtained using electrochemical test methods, namely LPR, EIS and potentiodynamic polarization. By running EIS alongside the more rapid LPR method, some additional information could be obtained to help understand the kinetics of the passivation process of mild steel in MKPC solutions. EIS can also address some shortcomings of LPR particularly in highly passive systems [34]. Potentiodynamic polarization was used to experimentally determine various corrosion related parameters such as the corrosion potential and pitting potential.

To facilitate the electrochemical measurements, a special three-electrode cell, consisting of mild steel as the working electrode, Ag/AgCl as the reference electrode and stainless steel as the counter electrode, was designed and manufactured for this study (Fig. 3). In this configuration, the reference electrode was placed near the working electrode to minimize the IR drop. The surface area of the mild steel that was exposed to the pore solution is 0.19 cm^2. In order to avoid crevice corrosion, a Teflon washer was tightly held to the surface of the mild steel by a screw, as shown in Fig. 3.

It should be noted that the surface area of the counter electrode was designed to be larger than that of the working electrode to ensure that a lower current density was maintained at the counter electrode. In this way, the counter electrode would not limit the current to the working electrode during polarization experiments [35, 36].

For testing the passivation in pore solutions, a mild steel pellet was used as the working electrode (as shown in Fig. 3). The pellets were obtained by cutting mild steel bar of Φ 16 mm into 10 mm-long pieces. The cross sections of the top and bottom surfaces of each pellet was polished sequentially using sand papers of grit 100, 400, 800, 1200 and 3000 which were then cleaned with deionized water and acetone. After polishing, the pellets were immediately inserted into the side wall of the cell as shown in Fig. 3. The cell was then filled with the pore

solution extracted from the MKPC or PC pastes. Prior to testing, the mild steel pellets were allowed to be stabilized in the pore solution for 15 minutes in the cell. The initial electrochemical measurements were then undertaken in a constant temperature room at 20°C. Following this the specimens were then stored at 20°C until testing began again at ages of 1, 3 and 7 days. All electrochemical measurements were performed using a "Gill AC" potentiostat (ACM Instruments UK). LPR measurements were carried out using a potentiodynamic sweep from -15 mV to 15 mV relative to the reference potential at a sweep rate of 0.166 mV/s. EIS measurements were performed using an applied AC signal with amplitude 32 mV over a frequency range of 100 kHz - 0.01 Hz. Fitting of EIS data was carried out using the ZSimpWin software. Potentiodynamic polarization experiments were executed using a sweep rate of 0.16 mV/s over a sweep range of -1.2 V - 1.2 V

2.5.3 Characterisation of the composition of passive film

2.5.3.1 X-ray photoelectron spectroscopy

Surface composition analysis was conducted by XPS to characterise the chemical composition of the passive film formed on the specimens immersed in the pore solution for 3 hours. The short period of immersion was adopted here to avoid the precipitation of KH_2PO_4 (from the MKPC pore solutions) on the passive film, which could significantly cover the passive film formed underneath. High resolution X-ray photoelectron spectra were obtained with a Thermo Scientific K-alpha photoelectron spectrometer using monochromatic Al−Kα radiation (1486.6 eV). Prior to the XPS experiments, the mild steel specimens were cleaned with deionized water in an ultrasonic bath and subsequently cleaned in acetone to remove contaminants from the specimen surface. During the XPS measurement, the pressure was set at approximately 4×10^{-7} mbar in the analysis chamber. Survey scans were collected in the range of 0~1100 eV (binding energy). The high-resolution spectra of O 1s, Fe 2p and P 2p were then measured. To obtain the depth profile, the surface was etched with Ar+ ions at 3.0 keV and 10 mA for 5 seconds before each scan. The binding energies of the measured

XPS spectra were calibrated by the C 1s peak (284.6 eV) and analysed using the CasaXPS software. The XPS spectra of O 1s, Fe 2p and P 2p XPS were fitted with a Shirley background, and the line shapes were deconvoluted by an asymmetric Gaussian-Lorentzian sum function.

2.5.3.2 Raman spectroscopy

Raman spectroscopy was used to complement XPS for further identification of the chemical composition in the passive film. As a vibrational spectroscopy, Raman spectroscopy can provide 'fingerprint' information of molecular structures and, therefore, can clearly identify the corrosion products formed as well as their molecular structure. The same specimens as those used for XPS were employed in the Raman measurements. *Ex situ* Raman spectra of the passive film were obtained via a Renishaw 2000 micro-Raman spectrometer with a sensitive CCD detector coupled to a microscope for a point-by-point analysis. The laser was focused on the specimens via a Leica 50× (NA = 0.50) into a spot size of Φ 1.4 μm. The laser power, operating at a wavelength of 514.5 nm, was controlled at around 0.73 mW in order to reduce the heat generated during the Raman analysis. This is needed because the iron oxide and hydroxide are known to be sensitive to thermal effects. Thus, using the low laser power can ensure the reliability of the data. The spectra were recorded with an exposure time of 60 seconds and 5 accumulations to improve the signal-to-noise ratio (SNR).

3 Results and discussion

3.1 pH and composition of MKPC pore solutions

The results for pH and the concentration of phosphate ions, determined for each of the MKPC pore solutions, are presented in Fig. 4. The initial pH values of the MKPC pore solutions are all very low while the concentrations of phosphate ions are quite high, which is attributed to the release of protons from KH_2PO_4 in water: $KH_2PO_4 \rightarrow K^+ + H^+ + HPO_4^-$ [37]. At the age of 1 day, the measured pH values of all the MKPC pore solutions significantly increased while the concentration of phosphate ions decreased when compared with those detected immediately

after mixing. This is due to the increased consumption of KH_2PO_4 with the development of the hydration process. Moreover, the pore solution of M/P 7 at 1 day is weakly alkaline (pH 8.7), whereas much higher pH values were obtained for the pore solution of M/P 12 (pH 10.1) and M/P 17 (pH 10.9). On the other hand, the concentration of phosphate ions of the pore solution of M/P 7 (1.5×10^5 ppm) is significantly higher than that of M/P 12 (7.8×10^4 ppm) and M/P 17 (2.6×10^2 ppm).

3.2 Passivation behaviour of mild steel in MKPC pore solutions

3.2.1 Linear polarization resistance measurements

The values of polarization resistance (R_p), calculated from linear polarization resistance (LPR) measurements of the mild steels in MKPC and PC pore solutions, are presented in Fig. 5. It can be observed that R_p rises to higher values over the exposure period in both the MKPC and PC pore solutions [38, 39]. In addition, the measured R_p values of the mild steels in the MKPC pore solutions increased with an increase in M/P ratio during the whole immersion period, suggesting that the steel passivity increased with the increase in M/P ratio, i.e. a higher M/P favours the formation of the protective passive film on the mild steel. Furthermore, it seems that the passivity of mild steel in the PC pore solution, based on the LPR results, is higher than mild steel in MKPC pore solutions of M/P 7 and 12 over the whole immersion period. However, it is understood that R_p could be underestimated when using the LPR method in a highly passivated system [34]. Therefore, EIS, arguably a more accurate method for highly passivated systems, was also employed in this study.

3.2.2 Electrochemical impedance spectroscopy

EIS spectra were collected on day 0 (i.e. immediately after immersing the mild steel in the pore solutions) and 7 days in the MKPC and PC pore solutions (Fig. 6). Among these spectra, Figs. 6a and 6c represent the Nyquist plots of EIS data at 0 and 7 days respectively, whilst Figs. 6b and 6d show the Bode plots accordingly.

As can be noticed from Figs. 6a and 6c, the semi-circle diameter of the Nyquist plots, which indicates the polarization resistance of the mild steel, is observed to be higher in all the MKPC specimens than that of the PC specimen, suggesting that higher passivity is obtained in the MKPC pore solutions than that in the PC pore solution. Moreover, the semi-circle diameter also increases with the increase in M/P ratio at both 0 and 7 days, as shown in Figs. 6a and 6c, indicating that the passivity of the mild steel increases with an increasing M/P. In addition, it was found that the semi-circle diameter increased markedly in both MKPC and PC pore solutions at 7 days when compared with those at day 0. This implies that the corrosion resistance increases over time, which is consistent with the LPR results shown in Fig. 5. Additionally, as shown in Figs. 6b and 6d, all the MKPC specimens exhibited a broader and higher Bode phase peak compared with that of the PC specimen. This could be attributed to the existence of an adsorption layer on top of the steel surface in the MKPC pore solutions, which is similar to those phenomena observed when a corrosion inhibitor is introduced during the passivation process [40].

To identify the passive film resistance and the charge transfer resistance at the mild steel/electrolyte interface, a suitable equivalent element circuit (EEC) was chosen. Generally, the number of the resistance-capacitance (RC) elements in EECs relate to the main peaks identified in the Bode plots [41]. Based on the broad Bode peak observed in the MKPC pore solutions, an EEC model with two RC elements (Fig. 7) was found to represent the EIS data with a chi-squared value of 10^{-3} or even lower (suggesting a good fitting) [42, 43]. In the resultant EEC model (Fig. 7), R_s corresponds to the solution resistance while R_f and Q_f can be attributed to the resistance and capacitance of the passive film formed on the metallic surface, respectively. In addition, R_{ct} and Q_{ct} are considered to be the charge transfer resistance and capacitance of the double layer at the mild steel/electrolyte interface, respectively. It should be noted that a constant phase element (CPE) was adopted for Q_f and Q_{dl} in the EEC model as shown in Fig. 7 to replace the ideal capacitance. This is because, compared to the ideal capacitance, the CPE can reflect the phenomenon existing in the real

situation, such as the non-homogeneity from the irregularities on the steel surface, surface roughness and fractal surface [44].

The evolution of the R_f and R_{ct} values obtained from the EIS fitting is presented in Fig. 8. It is observed that both the R_f and R_{ct} of the MKPC specimens are always higher than those of the corresponding PC specimen during the whole immersion period. This is indicative of the formation of more protective passive films in the MKPC pore solutions than in the PC pore solution, which is possibly associated with the interaction between the mild steel and anions in the MKPC pore solutions, such as phosphate ions. The detailed information is further presented in the following sections. Additionally, it can be noticed that the R_f and R_{ct} in the MKPC pore solutions always increase with an increasing M/P ratio over the exposure period, which suggests that the M/P ratio has a significant influence on the properties of the passive film formed. Furthermore, the R_f and R_{ct} in M/P 7 pore solution are markedly lower than those in M/P 12 and 17 pore solutions. This indicates that the passivation process in M/P 7 pore solution could be distinctively different from those in M/P 12 and 17 pore solutions, which will be discussed further below.

3.2.3 Potentiodynamic polarization measurements

The potentiodynamic polarization curves of the mild steel in the MKPC and PC pore solutions are shown in Fig. 9. The corresponding electrochemical parameters, including open circuit potential E_{corr} and pitting potential E_{pit}, were obtained and are listed in Table 4.

It can be observed from Table 4 that, with the increase of the M/P ratio, the corrosion potential (E_{corr}) increases, indicating that the passivity of the mild steel increases with an increase in the M/P ratio. Moreover, when compared to the PC specimen, all the MKPC specimens exhibited lower cathodic current densities i_c in the whole cathodically polarized region and lower anodic current densities i_a in the anodically polarized region from -500 mV to 1000 mV. This could imply that the phosphate ions might have played an inhibiting role in both anodic and cathodic processes in all the MKPC pore solutions, leading to the formation of a more protective passive

film. Similar observations and conclusions have also been reported in the literature [45].

Additionally, for the MKPC specimens, some distinguishable patterns of the polarization curves at the anodic potential range can be recognized in Fig. 9. At a low anodic potential range, the polarization scan of the mild steel in the M/P 7 specimen produced the highest anodic current among the three M/P ratios, which indicates that the least protective passive film has been formed on the mild steel in the M/P 7 specimen. However, when the anodic potential was applied to a higher range, the anodic current of the mild steel in the M/P 7 pore solution was reduced to the lowest value. This could be attributed to the preferential precipitation of insoluble iron phosphate on the passive film of the mild steel in the M/P 7 specimen, which could inhibit any further ion dissolution through the passive film [46]. In comparison, an opposite trend can be observed from the M/P 12 and 17 specimens, that is, the anodic current increased with the increase of the anodic potential at both low and high anodic potential ranges, which presumably owes to the lower concentration of phosphate ions (as shown in Fig. 4) in both M/P 12 and 17 pore solutions compared to that of M/P 7, leading to a reduction in the precipitation of iron phosphate.

3.3 Chemical composition of the passive film formed in MKPC pore solutions

3.3.1 X-ray photoelectron spectroscopy

The XPS was conducted to characterize the chemical composition of the passive film. The XPS signals obtained from the surface region of the passive film in different MKPC pore solutions are presented in Fig. 10. Table 5 summarizes the binding energies of each of the possible species to be occurred in this study according to the previous literature [46-49]. As shown in Fig. 10, the deconvoluted Fe $2p_{3/2}$ spectra exhibit peaks which could be assigned to Fe^0, Fe(II) species (such as FeO and Fe_3O_4), Fe(III) species (like Fe_2O_3 and FeOOH) as well as the Fe(II) satellite. Additionally, the main O species, such as O^{2-}, OH^- and PO_4^{3-}, are also

identified. In terms of the P element, the P 2p peak could only be attributed to PO_4^{3-} because in the current study KH_2PO_4 was the only phosphate introduced into the system.

To identify the possible iron compounds formed during the passivation process and thus to understand the role of phosphate ions in the passivation process at different M/P ratios, the $P/(Fe^{3+}+Fe^{2+})$ ratios in the surface region of the passive film were calculated based on the results in Fig. 10. The calculated $P/(Fe^{3+}+Fe^{2+})$ ratios are then plotted against the depth of the passive film in Fig. 11. As expected, the $P/(Fe^{3+}+Fe^{2+})$ ratio of the M/P 7 specimen is significantly higher than those of the M/Ps 12 and 17 specimens at all the depths, which suggests that significant precipitation of iron phosphate occurred in the passive film of the M/P 7 specimen. In addition, the $P/(Fe^{3+}+Fe^{2+})$ ratio of M/P 7 significantly decreases when the passive film was sputtered, which indicates that phosphate ions might mainly precipitate in the outermost layer of the passive film of the M/P 7 specimen. On the other hand, an extremely low $P/(Fe^{3+}+Fe^{2+})$ ratio was identified from the M/P 17 specimen, indicating that few phosphate-containing compounds formed on the M/P 17 specimen. It should be noted that even the $P/(Fe^{3+}+Fe^{2+})$ ratio of the M/P 7 specimen is lower than that of the stoichiometrical ratio of $Fe_3(PO4)_2{\cdot}nH_2O$ (P/Fe^{2+} =0.67), indicating that other species, such as iron oxides/hydroxides, could also exist in the passive film formed in the MKPC pore solutions.

To clarify the existence of iron oxide or hydroxide in the passive film formed in the pore solution of MKPC, the OH^-/O^{2-} ratios in the passive films formed in the pore solutions of different M/P ratios are also presented in Fig. 12. It can be seen that the OH^-/O^{2-} ratio decreases with increasing depth of the passive film for all the M/P ratios, which suggests that iron hydroxide is mainly formed in the outer layer of the passive film while iron oxide mainly dominates the inner layer of the passive film. This result is consistent with the previous studies reported in the literature which showed that the passive film of mild steel mainly consists of an outer layer of porous FeOOH, and an inner layer of compact Fe_2O_3 or Fe_3O_4/FeO [50, 51].

To further verify the possible chemical composition of the passive film formed in different MKPC pore solutions, the Fe^{2+}/Fe^{3+} ratios in the passive film were calculated from the XPS

spectra (as shown in Fig. 10) and the results are presented against the depth of passive film in Fig. 13. It can be observed that Fe^{2+}/Fe^{3+} ratios increased with the passive film depth for all the MKPC specimens. Similar trends have also been reported by other researchers showing that the inner layer of the passive film mainly consists of Fe(II) oxides while the outer layer is usually dominated by Fe(III) oxides [2, 3]. Known that OH^-/O^{2-} ratio decreases with passive film depth, it can be deduced that Fe(III) hydroxide forms mostly in the outermost part while the amount of Fe(II) oxide increases in the inner part of passive film for MKPC specimens [3]. In addition, the Fe^{2+}/Fe^{3+} ratios increased with the increase of the M/P ratios in the inner part of the passive films. As the pH increased with the increase of M/P, this trend can be well supported by the literature which showed that the higher the pH is, the higher the Fe^{2+}/Fe^{3+} ratio should be [7]. More importantly, it should be noted that, as a higher Fe^{2+}/Fe^{3+} ratio would result in higher passivity of steel [41], the current results would suggest that a higher M/P can increase the passivity of the mild steel in MKPC cement, which also can be well corroborated by the electrochemical results presented before.

On the contrary, an opposite trend was observed from the outermost layer of passive film, i.e. with the increase of the M/P ratio, the Fe^{2+}/Fe^{3+} ratio decreased. This indicates that unlike with what happened in the inner layer, the pH is no longer the dominating factor for determining the composition of the outermost layer of passive film. Instead, the decreasing Fe^{2+}/Fe^{3+} ratio in the outermost layer with the increase of the M/P ratio could be related to the precipitation of iron phosphate. As it has been well established, in the presence of O_2 and H_2O, Fe^{2+} should be formed in the solution (as shown in Eqs. 2-3). Since the solubility of $Fe_3(PO_4)_2$ (2.47×10^{-8} M) is much lower than that of $Fe(OH)_2$ (3.16×10^{-6} M) at a low pH (between 6 and 8) [52], the dissolved Fe^{2+} from the steel substrate would preferably react with PO_4^{3-} to precipitate $Fe_3(PO_4)_2$ (Eq. 4), rather than the formation of $Fe(OH)_2$ with OH^- (Eq. 5). Moreover, the Gibbs free energy of $Fe_3(PO_4)_2$ (–2444.80 kJ/mol) is lower than that of $FePO_4$ (-1657.70 kJ/mol) [53, 54], which hinders the oxidation of $Fe_3(PO_4)_2$ into $FePO_4$ during the passivation process. As shown in Fig. 4, the concentration of phosphate ions of the 1-day MKPC pore solutions

decreased significantly with an increase of M/P ratios, in which case the highest phosphate concentrations occurred at M/P 7 ($1.5x10^5$ ppm) while the lowest at M/P 17 ($2.57x10^2$ ppm). Therefore, it can be deduced that the precipitation of $Fe_3(PO_4)_2$ should be the dominant reaction at the outermost layer of the mild steel in M/P 7. In the case of M/P 17, due to the much reduced phosphate content, the formation of $Fe_3(PO_4)_2$ is significantly reduced. Instead, the combination of Fe^{2+} and OH^- into $Fe(OH)_2$ precipitates is favoured, which eventually leads to increased formation of Fe(III) oxide or hydroxide in the outermost layer of the passive film in the presence of oxygen, as shown in Equations. 5-8. Additionally, as indicated in Fig. 4, with the increase of M/P from 7 to 17, the pH of the pore solution increased from pH 8.7 to 10.9, which also favours the precipitation of iron oxides/hydroxides in M/P 17 (further details are given in Section 3.4 and the Raman results below can further support this hypothesis). This may explain why the Fe^{2+}/Fe^{3+} ratio in the outermost layer of the passive film decreases with increasing M/P ratios as shown in Fig. 13.

$$Fe \rightarrow Fe^{2+}(aq) + 2e^- \quad \text{Eq. 2}$$

$$O_2 + 2H_2O + 4e^- \rightarrow 4OH^-(aq) \quad \text{Eq. 3}$$

$$3Fe^{2+}(aq) + 2PO_4^{3-}(aq) + nH_2O \rightarrow Fe_3(PO_4)_2 \cdot nH_2O(s) \quad \text{Eq. 4}$$

$$Fe^{2+}(aq) + 2OH^-(aq) \rightarrow Fe(OH)_2(s) \quad \text{Eq. 5}$$

$$4Fe(OH)_2(s) + O_2 + 2H_2O \rightarrow 4Fe(OH)_3(s) \quad \text{Eq. 6}$$

$$Fe(OH)_3(s) \rightarrow FeOOH(s) + H_2O \quad \text{Eq. 7}$$

$$2Fe(OH)_3(s) \rightarrow Fe_2O_3(s) + 3H_2O \quad \text{Eq. 8}$$

3.3.2 Raman spectroscopy

Built upon the chemical elements identified from XPS, the Raman spectroscopy was employed to recognize the chemical compounds formed in the passive films and the results are presented in Fig. 14. It can be seen that in the spectra of M/P 12 and 17 specimens, two peaks can be observed at around 223 cm^{-1} and 293 cm^{-1}, which could be respectively assigned to

the Fe-O symmetric stretching and Fe-OH symmetric bending vibrations. In addition, peaks have also been identified at 410 cm^{-1} and 546 cm^{-1}, which can be attributed to two Fe-OH asymmetric stretching modes [55, 56]. From the above four vibration modes, it can be deduced that goethite (α-FeOOH) has been formed in the passive film [12, 57]. On the other hand, Raman peaks at around 665 cm^{-1} and 745 cm^{-1} can also be observed in the specimens of M/Ps 12 and 17, which can be attributed to the stretching vibration modes along the Fe-O bond of maghemite (γ-Fe_2O_3) [57]. As Raman spectroscopy can only detect the surface region of the passive film, Raman results shown in Fig. 14 would imply that the outermost part of the passive film of M/Ps 12 and 17 mainly consists of γ-Fe_2O_3 and α-FeOOH, which is consistent with XPS results showing that the outermost part of the passive films of M/Ps 12 and 17 mainly contains Fe(III) ion.

In contrast, all the above Raman peaks of M/Ps 12 and 17 were not detected in the specimen of M/P 7. Instead, peaks at 439 cm^{-1}, 585 cm^{-1} and 944 cm^{-1} were detected in the M/P 7 specimen, which can be assigned to the v_2 symmetric bending mode, v_4 symmetric bending mode and v_1 symmetric stretching mode of PO_4, respectively [58]. This would indicate that, compared to M/Ps 12 and 17 which mainly consists of γ-Fe_2O_3 and α-FeOOH, the passive film of M/P 7 could be mainly dominated by iron phosphates.

To compare the passive film formed in PC with those in MKPC, Fig. 15 shows the Raman spectrum of the mild steel immersed in PC pore solution. As can be seen, only one Raman peak can be noticed at 665 cm^{-1}, which corresponds to the symmetric stretching vibration of oxygen atoms along the Fe-O bonds in the T sites of Fe_3O_4. This indicates that the passive film of the PC specimen only consists of magnetite (Fe_3O_4), which is consistent with the previous literature [2, 59].

3.4 Passivation mechanism of the mild steel in MKPC pore solutions

As highlighted before, to form a good quality passive film, it is generally believed that a pH value above 10.5 is essential and generally the higher the pH is, the better the quality of the

passive film [7]. In this study, the measured pH values range from only 8.7 to 10.9 for the MKPC specimens. Therefore, a reduced quality of the passive film should have been anticipated. However, the passivity of the mild steel in the MKPC pore solutions are demonstrated to be comparable or even higher than that in the PC pore solution according to the electrochemical results. As indicated in Figs. 11 and 14, the iron phosphates have been clearly identified, particularly in the outermost layer of the passive film formed in M/P 7. Therefore, the improved passivity could be attributed to the presence of phosphate ions, which is consistent with those hypotheses proposed in the literature [9, 60, 61]. Nonetheless, from the electrochemical results (such as Fig. 8b), it seems that pH has also played an important role in the passivity of mild steel, in a similar way as it has played in the PC system. It thus becomes evident that both pH and phosphates are key factors which determine the passivation of mild steel in the MKPC pore solutions.

To clearly understand the possible coupled effects of pH and phosphate, the Pourbaix diagram of the Fe-P-O system at 20 °C is drawn and shown in Fig. 16. It should be noted that this diagram can only be used to identify the possible stable equilibrium phases of an aqueous electrochemical system from a thermodynamic point of view, which does not account for the kinetic effects [62]. In Fig. 16, the solid lines separate the stable regions for Fe-P-O species. In addition, the vertical highlighted area represents the pH range of the MKPC solutions investigated in this study, while the horizontal blue dashed line indicates the standard electrode potential of iron. Therefore, according to Fig. 16, it is apparent that the following products could be formed at the standard electrode potential of iron: i) no stable precipitate exists below pH 3, ii) $Fe_3(PO_4)_2 \cdot 8H_2O$ precipitates between pH 3 and pH 8.8, and iii) Fe_3O_4 or FeOOH forms above pH 8.8. Based on this, the formation of stable iron phosphate is favoured for M/P 7 which has a low pH (8.7), while only iron oxide or hydroxide is favoured when the M/P is 12 (pH 10.1) or 17 (pH 10.9). This prediction is not only consistent with the XPS and Raman results obtained from the surface region of the passive films in this study but can also be corroborated by literature. For example, Smialowska and Staehle found that, depending

519 on the pH value of the phosphate-containing solutions, the passive film formed at pH 12.3
520 mainly consisted of iron oxides, while at pH 7 and 9.1, the passive film was mainly dominated
521 by phosphate compounds [63].

522 However, it should be noted that although the thermodynamic information, such as that shown
523 in Fig. 16, can give some useful information on the possible composition of the passive film,
524 in practice, the composition of passive film could differ from those predicted by the Pourbaix
525 diagram [64, 65]. This is because passivation is a kinetic process which involves dissolution,
526 diffusion and precipitation during the reactions with mild steel [66], which is not an equilibrium
527 process. This may well explain the slight differences identified in the composition of the
528 passive film between those predicted from Fig. 16 and the results obtained in Figs. 11-14.

529 Nevertheless, by taking account of the experimental data and the theoretical thermal dynamic
530 analysis mentioned above, two possible mechanisms involved in the passivation of mild steel
531 in MKPC have been proposed and these are schematically shown in Fig. 17. As illustrated in
532 Fig. 17, depending on the pH of the MKPC pore solutions, different passivation mechanisms
533 could dominate. When the pH is lower than 8.8 (such as the pH obtained from M/P 7), the
534 outermost layer is mainly composed of iron phosphate and iron hydroxide (Fig. 17a). On the
535 contrary, when the pH is higher than 8.8, γ-Fe_2O_3 and α-FeOOH are the dominant compounds
536 formed in the outermost layer of passive film (as exemplified by M/Ps 12 and 17). In terms of
537 the inner layer, regardless of the pH value, iron hydroxide or iron oxide could be the main
538 composition, as shown in Fig. 17a and Fig. 17b. Specifically, when the pH is low (e.g. lower
539 than 8.8 in the current study for M/P 7), the inner layer of the passive film consists of mainly
540 Fe(III) hydroxide (as shown in Fig. 17a), while Fe(II) oxide mainly dominates when pH is higher
541 than 8.8 (such as M/Ps 12 and 17) (Fig. 17b). This proposed composition of the inner layer is
542 consistent with the previous literature which showed that a low pH led to the formation of Fe(III)
543 oxide/hydroxide, while a high pH favoured the formation of Fe(II) oxide/hydroxide [3, 7]. Since
544 the protection provided by the passive film is mainly controlled by the inner layer [67], the
545 passivation degree of mild steel in MKPC should therefore be primarily determined by the

546 quality of iron oxide/hydroxide in the passive film, i.e., the inner layer of the passive films
547 formed in the MKPC pore solutions. As it has been reported that Fe(II) oxide formed in the
548 passive film can provide better protection to steel than Fe(III) hydroxide [68], it can thus be
549 deduced that the passive film shown in Fig. 17 b (i.e. for M/Ps 12 and 17) should produce
550 better passivity than that of Fig. 17 (a) (i.e. for M/P 7). Clearly, this deduction can be fully
551 supported by the electrochemical results shown in Figs. 5-9. Additionally, this can also be
552 corroborated by the previous studies reported in the literature showing that the passivity of
553 iron increases with pH in phosphate-containing solutions [63, 69].

554 On the other hand, it has been well established that the phosphate ion can be a good inhibitor
555 by forming some insoluble ferrous phosphate compounds [12] or by adsorbing [70] on the
556 steel surface, which inhibits any further corrosion process. In the current study, the formation
557 of iron phosphates has been clearly identified and this has been presented in Fig. 17a in the
558 proposed mechanism related to a low pH MKPC system. The unexpected good passivity from
559 M/P 7 (as shown in Fig. 17a) can thus be attributable to the inhibiting role played by the iron
560 phosphate on the outermost surface of the passive film. However, it should be noted that
561 regardless of the M/P, the adsorption of phosphate ions on the surface of the passive film [70,
562 71] could also have played an important role in enhancing the passivity of mild steel in the
563 MKPC system, leading to the much improved passivity compared to that in the PC system,
564 even though the pH values of MKPC are much lower than PC. Overall, it can be concluded
565 that both pH and phosphate contents are key factors influencing the passivation of mild steel
566 in the MKPC system, with pH dominating the degree of passivation. In other words, the
567 passivity of the mild steel in MKPC is to be mainly controlled by the M/P ratio. Therefore,
568 special attention should be paid to the M/P ratios when MKPC reinforced concretes are to be
569 designed for different exposure classes in order to ensure not only the strength, but also the
570 durability performance can meet the specific requirements.

4 Conclusions

In this paper, to investigate the passivation behaviour of mild steel in the MKPC pore solutions with different M/P ratios, a combination of electrochemical and materials characterisation techniques was used. Based on the data obtained, the following conclusions can be drawn:

1) Despite the low pH of the MKPC pore solution, the results from a detailed electrochemical study have demonstrated that the protective passive film can be formed on the surface of mild steel in all the MKPC pore solutions investigated. The passivity of the mild steel in MKPC was found to be comparable or even better than that formed in a conventional PC pore solution.
2) The M/P ratio has a significant influence on the passivity of mild steel. The passivation degree remarkedly increases with increasing M/P ratio from 7 to 17.
3) The passive film formed in the MKPC with M/P 7 consists of an outermost layer of iron phosphate and iron hydroxide, and an inner layer of mainly Fe(III) hydroxide, while those formed in M/P 12 and 17 are made up of an outermost layer of γ-Fe_2O_3 and α-FeOOH and an inner layer of Fe(II) oxide.
4) The passivation of mild steel in the MKPC pore solutions is mainly controlled by both the concentration of phosphate ions and the pH of the MKPC pore solutions. Phosphate ions improve the passivity through the precipitation of iron phosphates (as shown in M/P 7) as well as the possible adsorption of phosphate ions on the surface of mild steel. On the other hand, similar to its effect on the passivation of mild steel in a PC system, the pH of the MKPC pore solutions plays a dominant role on the degree of the passivation of mild steel in MKPC, with M/P 17 showing the most favourable influence on the passivity of mild steel due to its highest pH.

6. Acknowledgements

The authors are most thankful for the financial supports received for this research from UK Engineering and Physical Sciences Research Council (EPSRC) (Grant No. EP/M003159/1)

and National Natural Science Foundation of China (NSFC) (51461135003) under the EPSRC-NSFC Collaborative Research Scheme on ‘Sustainable Materials for Infrastructure’. The China Scholarship Council and UCL Faculty of Engineering Sciences are gratefully acknowledged for providing the studentship for Miss Danqian Wang’s PhD study at UCL. Mr Warren Gaynor, Dr Shi Shi and Dr Judith Zhou at UCL and Mr Fengrui Zhang from Chongqing University are also gratefully acknowledged for their help with the experimental work.

Data availability

The raw/processed data required to reproduce these findings cannot be shared at this time as the data also forms part of an ongoing study.

References

[1] J.V. Custódio, S.M.L. Agostinho, A.M.P. Simões, Electrochemistry and surface analysis of the effect of benzotriazole on the cut edge corrosion of galvanized steel, Electrochimica Acta, 55 (2010) 5523-5531.

[2] S. Joiret, M. Keddam, X.R. Nóvoa, M.C. Pérez, C. Rangel, H. Takenouti, Use of EIS, ring-disk electrode, EQCM and Raman spectroscopy to study the film of oxides formed on iron in 1 M NaOH, Cement and Concrete Composites, 24 (2002) 7-15.

[3] P. Ghods, O.B. Isgor, J.R. Brown, F. Bensebaa, D. Kingston, XPS depth profiling study on the passive oxide film of carbon steel in saturated calcium hydroxide solution and the effect of chloride on the film properties, Applied Surface Science, 257 (2011) 4669-4677.

[4] P. Ghods, O.B. Isgor, G. McRae, T. Miller, The effect of concrete pore solution composition on the quality of passive oxide films on black steel reinforcement, Cement and Concrete Composites, 31 (2009) 2-11.

[5] G.Y. Koga, B. Albert, V. Roche, R. Pereira Nogueira, On the intrinsic passivating ability of Belite-Ye’elimite-Ferrite towards carbon steel: A straightforward comparison with ordinary Portland cement, Corrosion Science, (2018).

[6] Y.M. Tang, Y.F. Miao, Y. Zuo, G.D. Zhang, C.L. Wang, Corrosion behavior of steel in simulated concrete pore solutions treated with calcium silicate hydrates, Constr Build Mater, 30 (2012) 252-256.

[7] Z. Ai, J. Jiang, W. Sun, D. Song, H. Ma, J. Zhang, D. Wang, Passive behaviour of alloy corrosion-resistant steel Cr10Mo1 in simulating concrete pore solutions with different pH, Applied Surface Science, 389 (2016) 1126-1136.

[8] A. Köliö, M. Honkanen, J. Lahdensivu, M. Vippola, M. Pentti, Corrosion products of carbonation induced corrosion in existing reinforced concrete facades, Cement and Concrete Research, 78 (2015) 200-207.

[9] A. Mohagheghi, R. Arefinia, Corrosion inhibition of carbon steel by dipotassium hydrogen phosphate in alkaline solutions with low chloride contamination, Construction Building Materials, 187 (2018) 760-772.

[10] S.M. Abd El Haleem, S. Abd El Wanees, E.E. Abd El Aal, A. Diab, Environmental factors affecting the corrosion behavior of reinforcing steel II. Role of some anions in the initiation and inhibition of pitting corrosion of steel in $Ca(OH)_2$ solutions, Corrosion Science, 52 (2010) 292-302.

[11] L. Dhouibi, E. Triki, A. Raharinaivo, G. Trabanelli, F. Zucchi, Electrochemical methods for evaluating inhibitors of steel corrosion in concrete, British Corrosion Journal, 35 (2000) 145-149.

[12] L. Yohai, W. Schreiner, M. Vázquez, M.B. Valcarce, Phosphate ions as effective inhibitors for carbon steel in carbonated solutions contaminated with chloride ions, Electrochimica Acta, 202 (2016) 231-242.

[13] Q. Yang, B. Zhu, X. Wu, Characteristics and durability test of magnesium phosphate cement-based material for rapid repair of concrete, Materials and Structures, 33 (2000) 229-234.

[14] S.A. Farrington, Rapid setting, high early strength binders, in, U.S. Patent, Washington, DC, 2000.

[15] H. Ma, B. Xu, Z. Li, Magnesium potassium phosphate cement paste: Degree of reaction, porosity and pore structure, Cement and Concrete Research, 65 (2014) 96-104.

[16] H. Ma, B. Xu, J. Liu, H. Pei, Z. Li, Effects of water content, magnesia-to-phosphate molar ratio and age on pore structure, strength and permeability of magnesium potassium phosphate cement paste, Materials & Design, 64 (2014) 497-502.

[17] H. Ma, B. Xu, Potential to design magnesium potassium phosphate cement paste based on an optimal magnesia-to-phosphate ratio, Materials & Design, 118 (2017) 81-88.

[18] M. Le Rouzic, T. Chaussadent, L. Stefan, M. Saillio, On the influence of Mg/P ratio on the properties and durability of magnesium potassium phosphate cement pastes, Cement and Concrete Research, 96 (2017) 27-41.

[19] H. Lahalle, C. Cau Dit Coumes, A. Mesbah, D. Lambertin, C. Cannes, S. Delpech, S. Gauffinet, Investigation of magnesium phosphate cement hydration in diluted suspension and its retardation by boric acid, Cement and Concrete Research, 87 (2016) 77-86.

[20] T. Sugama, L.E. Kukacka, Characteristics of magnesium polyphosphate cements derived from ammonium polyphosphate solutions, Cement and Concrete Research, 13 (1983) 499-506.

[21] C. Qian, J. Yang, Effect of Disodium Hydrogen Phosphate on Hydration and Hardening of Magnesium Potassium Phosphate Cement, Journal of Materials in Civil Engineering, 23 (2011) 1405-1411.

[22] L. Chong, C. Shi, J. Yang, H. Jia, Effect of limestone powder on the water stability of magnesium phosphate cement-based materials, Construction Building Materials, 148 (2017) 590-598.

671 [23] L. Chong, J. Yang, C. Shi, Effect of curing regime on water resistance of magnesium–
672 potassium phosphate cement, Construction Building Materials, 151 (2017) 43-51.

673 [24] G. Zhang, G. Li, T. He, Effects of sulphoaluminate cement on the strength and water
674 stability of magnesium potassium phosphate cement, Construction and Building Materials,
675 132 (2017) 335-342.

676 [25] T. Zhang, H. Chen, X. Li, Z. Zhu, Hydration behavior of magnesium potassium phosphate
677 cement and stability analysis of its hydration products through thermodynamic modeling,
678 Cement and Concrete Research, 98 (2017) 101-110.

679 [26] H. Pei, Z. Li, J. Zhang, Q. Wang, Performance investigations of reinforced magnesium
680 phosphate concrete beams under accelerated corrosion conditions by multi techniques,
681 Construction Building Materials, 93 (2015) 989-994.

682 [27] J. Zhang, H. Ma, H. Pei, Z. Li, Steel corrosion in magnesia–phosphate cement concrete
683 beams, Magazine of Concrete Research, 69 (2017) 35-45.

684 [28] Chemically Bonded Phosphate Ceramics: More Than a Temporary Corrosion Covering,
685 Advanced Materials & Processes, 169 (2011) 2.

686 [29] M. Sari, E. Prat, J.F. Labastire, High strength self-compacting concrete Original solutions
687 associating organic and inorganic admixtures, Cement and Concrete Research, 29 (1999)
688 813-818.

689 [30] A. Princigallo, P. Lura, K. van Breugel, G. Levita, Early development of properties in a
690 cement paste: A numerical and experimental study, Cement and Concrete Research, 33 (2003)
691 1013-1020.

692 [31] P. Garcés, P. Saura, E. Zornoza, C. Andrade, Influence of pH on the nitrite corrosion
693 inhibition of reinforcing steel in simulated concrete pore solution, Corrosion Science, 53 (2011)
694 3991-4000.

695 [32] P. Longuet, La phase liquide du ciment hydraté, (1973).

696 [33] R.S. Barneyback, S. Diamond, Expression and analysis of pore fluids from hardened
697 cement pastes and mortars, Cement and Concrete Research, 11 (1981) 279-285.

698 [34] M. Kouřil, P. Novák, M. Bojko, Limitations of the linear polarization method to determine
699 stainless steel corrosion rate in concrete environment, Cement and Concrete Composites, 28
700 (2006) 220-225.

701 [35] P. Ducheyne, Comprehensive biomaterials, Elsevier, 2015.

702 [36] H.R. Luckarift, P.B. Atanassov, G.R. Johnson, Enzymatic fuel cells: From fundamentals
703 to applications, John Wiley & Sons, 2014.

704 [37] B. Xu, B. Lothenbach, A. Leemann, F. Winnefeld, Reaction mechanism of magnesium
705 potassium phosphate cement with high magnesium-to-phosphate ratio, Cement and Concrete
706 Research, 108 (2018) 140-151.

707 [38] J. Shi, J. Ming, W. Sun, Electrochemical performance of reinforcing steel in alkali-
708 activated slag extract in the presence of chlorides, Corrosion Science, (2018).

709 [39] J. Shi, J. Ming, M. Wu, Electrochemical behavior and corrosion products of Cr-modified
710 reinforcing steels in saturated $Ca(OH)_2$ solution with chlorides, Cement and Concrete
711 Composites, 110 (2020) 103587.

712 [40] U. Rammelt, S. Koehler, G. Reinhard, Synergistic effect of benzoate and benzotriazole
713 on passivation of mild steel, Corrosion Science, 50 (2008) 1659-1663.

714 [41] M.E. Orazem, B. Tribollet, Electrochemical impedance spectroscopy, John Wiley & Sons,
715 2017.

716 [42] G. Blanco, A. Bautista, H. Takenouti, EIS study of passivation of austenitic and duplex
717 stainless steels reinforcements in simulated pore solutions, Cement and Concrete Composites,
718 28 (2006) 212-219.

719 [43] V.A. Alves, C.M.A. Brett, Characterisation of passive films formed on mild steels in
720 bicarbonate solution by EIS, Electrochimica Acta, 47 (2002) 2081-2091.

721 [44] M. Criado, D.M. Bastidas, S. Fajardo, A. Fernández-Jiménez, J.M. Bastidas, Corrosion
722 behaviour of a new low-nickel stainless steel embedded in activated fly ash mortars, Cement
723 and Concrete Composites, 33 (2011) 644-652.

724 [45] L. Yohai, M.B. Valcarce, M. Vázquez, Testing phosphate ions as corrosion inhibitors for
725 construction steel in mortars, Electrochimica Acta, 202 (2016) 316-324.

726 [46] J. Benzakour, A. Derja, Characterisation of the passive film on iron in phosphate medium
727 by voltammetry and XPS measurements, Journal of Electroanalytical Chemistry, 437 (1997)
728 119-124.

729 [47] A. Grosvenor, B. Kobe, M. Biesinger, N. McIntyre, Investigation of multiplet splitting of Fe
730 2p XPS spectra and bonding in iron compounds, Surface and Interface Analysis, 36 (2004)
731 1564-1574.

732 [48] E. Ferreira, N. Oliveira, S. Biaggio, P. Nascente, R. Rocha-Filho, N. Bocchi, XPS
733 characterization of anodic oxides grown on biocompatible Ti–50Zr alloy in different acid
734 electrolytes, 38 (2006) 417-421.

735 [49] N. McIntyre, D. Zetaruk, X-ray photoelectron spectroscopic studies of iron oxides,
736 Analytical Chemistry, 49 (1977) 1521-1529.

737 [50] F. Miserque, B. Huet, G. Azou, D. Bendjaballah, V. L'Hostis, X-ray photoelectron
738 spectroscopy and electrochemical studies of mild steel FeE500 passivation in concrete
739 simulated water, J. Phys. IV France, 136 (2006) 89-97.

740 [51] L. Freire, X.R. Nóvoa, M.F. Montemor, M.J. Carmezim, Study of passive films formed on
741 mild steel in alkaline media by the application of anodic potentials, Materials Chemistry and
742 Physics, 114 (2009) 962-972.

743 [52] H.M. Azam, K.T. Finneran, Fe(III) reduction-mediated phosphate removal as vivianite
744 (Fe3(PO4)2·8H2O) in septic system wastewater, Chemosphere, 97 (2014) 1-9.

745 [53] J.A. Dean, Lange's handbook of chemistry, New york; London: McGraw-Hill, Inc., 1999.

746 [54] A.L. Iglesia, Estimating the thermodynamic properties of phosphate minerals at high and
747 low temperature from the sum of constituent units, Consejo Superior de Investigaciones
748 Científicas, 65 (2009) 109-119.

749 [55] M.A. Legodi, D. de Waal, The preparation of magnetite, goethite, hematite and maghemite
750 of pigment quality from mill scale iron waste, Dyes and Pigments, 74 (2007) 161-168.

751 [56] G. Nauer, P. Strecha, N. Brinda-Konopik, G. Liptay, Spectroscopic and thermoanalytical
752 characterization of standard substances for the identification of reaction products on iron
753 electrodes, Journal of thermal analysis, 30 (1985) 813-830.

754 [57] D. De Faria, S. Venâncio Silva, M. De Oliveira, Raman microspectroscopy of some iron
755 oxides and oxyhydroxides, Journal of Raman spectroscopy, 28 (1997) 873-878.

756 [58] R.L. Frost, M.L. Weier, K.L. Erickson, O. Carmody, S.J. Mills, Raman spectroscopy of
757 phosphates of the variscite mineral group, Journal of Raman Spectroscopy, 35 (2004) 1047-
758 1055.

759 [59] J. Gui, T.M. Devine, In situ vibrational spectra of the passive film on iron in buffered borate
760 solution, Corrosion Science, 32 (1991) 1105-1124.

761 [60] S.A.M. Refaey, Inhibition of steel pitting corrosion in HCl by some inorganic anions,
762 Applied Surface Science, 240 (2005) 396-404.

763 [61] N. Etteyeb, L. Dhouibi, H. Takenouti, M.C. Alonso, E. Triki, Corrosion inhibition of carbon
764 steel in alkaline chloride media by Na_3PO_4, Electrochimica Acta, 52 (2007) 7506-7512.

765 [62] B. Beverskog, I. Puigdomenech, Revised pourbaix diagrams for iron at 25–300 °C,
766 Corrosion Science, 38 (1996) 2121-2135.

[63] Z. Szklarska-Smialowska, R.W. Staehle, Ellipsometric Study of the Formation of Films on Iron in Orthophosphate Solutions, Journal of The Electrochemical Society, 121 (1974) 1393-1401.

[64] V.A.N. de Carvalho, R.A.d.S. Luz, B.H. Lima, F.N. Crespilho, E.R. Leite, F.L. Souza, Highly oriented hematite nanorods arrays for photoelectrochemical water splitting, Journal of Power Sources, 205 (2012) 525-529.

[65] Z. Ahmad, in: Principles of corrosion engineering and corrosion control, Butterworth-Heinemann, Oxford, 2006, pp. 9-56.

[66] J. Huang, X. Wu, E.-H. Han, Electrochemical properties and growth mechanism of passive films on Alloy 690 in high-temperature alkaline environments, Corrosion Science, 52 (2010) 3444-3452.

[67] D.D. Macdonald, Theory of Steady-State Passive Films, Journal of the Electrochemical Society, 137 (1990) 2395.

[68] N. Sato, T. Noda, K. Kudo, Thickness and structure of passive films on iron in acidic and basic solution, Electrochimica Acta, 19 (1974) 471-475.

[69] F. Zucchi, G. Trabanelli, Anodic behaviour of Fe in phosphate solutions, Corrosion Science, 11 (1971) 141-151.

[70] M. Reffass, R. Sabot, M. Jeannin, C. Berziou, P. Refait, Effects of phosphate species on localised corrosion of steel in $NaHCO_3$+NaCl electrolytes, Electrochimica Acta, 54 (2009) 4389-4396.

[71] T. Nishimura, T. Kodama, Clarification of chemical state for alloying elements in iron rust using a binary-phase potential–pH diagram and physical analyses, Corrosion Science, 45 (2003) 1073-1084.

Tables

Table 1 Chemical composition of PC (wt.%).

Oxides	**SiO_2**	**Al_2O_3**	**Fe_2O_3**	**CaO**	**MgO**	**K_2O**	**Na_2O**	**SO_3**
Content	23.00	6.15	2.95	61.30	1.80	0.68	0.22	2.50

Table 2 Chemical composition of mild steel (wt.%).

Composition	**%C**	**%P**	**%S**	**%Mn**	**%Si**	**%Cu**
Content	0.17	0.0047	0.017	0.46	0.26	0.019

Table 3 Mix design and batch weight of MKPC pastes.

Mix proportion			**Batch quantity - 1000 g powder**			
M/P	Borax	W/C	MgO	KDP	Borax	Water
7	15%	0.22	674.60	325.40	101.19	220
12	15%	0.22	780.41	219.59	117.06	220
17	15%	0.22	834.30	165.70	125.14	220

799 Table 4 The electrochemical parameters obtained from potentiodynamic polarization

800 curves.

Specimens	E_{corr} / mV	E_{pit} / mV
M/P 7	-871.15	891.47
M/P 12	-800.35	840.28
M/P 17	-532.62	861.98
PC	-481.59	629.60

801

802 Table 5 Estimated XPS peak positions of elements on the steel surface [46-49].

Peak	Component	Binding energy / eV	Ref.
Fe $2p_{3/2}$	Fe^{0}	706.8	[49]
	Fe^{2+}	709.0	[47]
	Fe^{3+}	711.2	[47]
	Fe^{2+} satellite	714.3	[47]
O 1s	O^{2-}	530.1	[47]
	OH^{-}	531.2	[47]
	PO_4^{3-}	533.0	[46]
P 2p	PO_4^{3-}	133.5	[48]

803

Figures

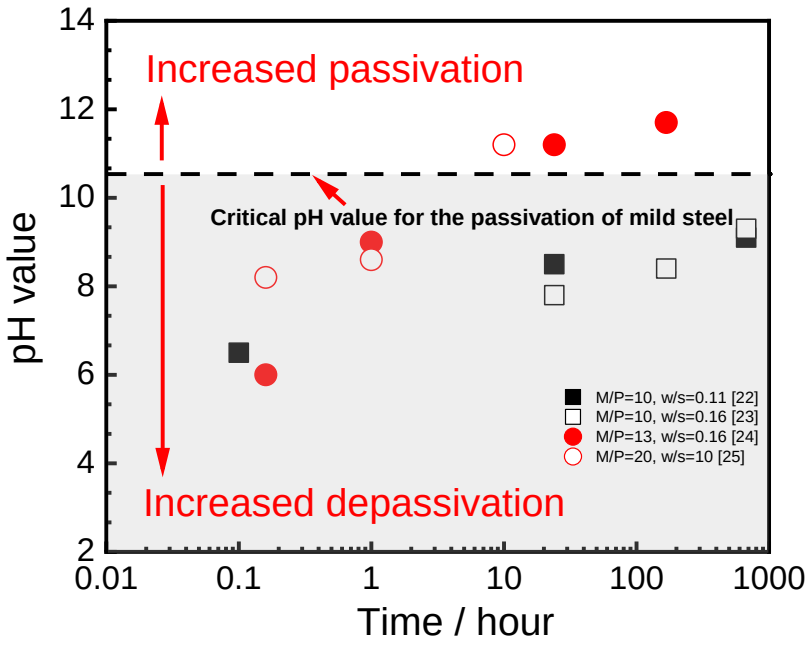

Fig. 1. The evolution of pH value of MPC pore solution with curing duration according to the previous literature (M/P is molar ratio).

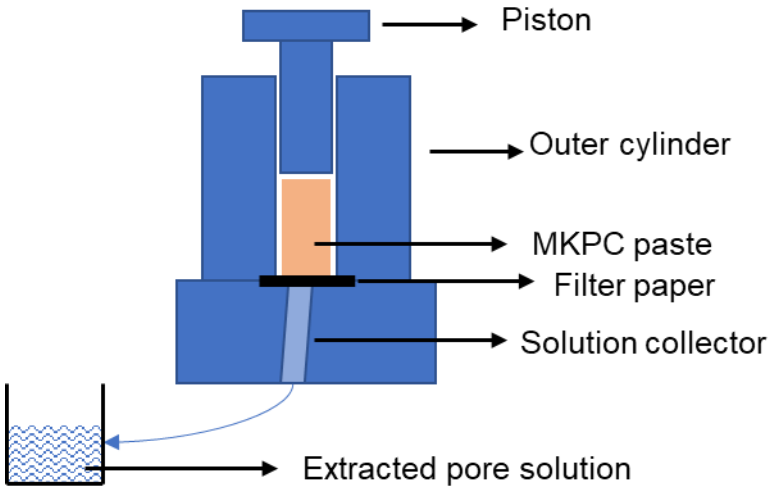

815

816 Fig. 2. Schematic diagram of pore solution extraction facility.

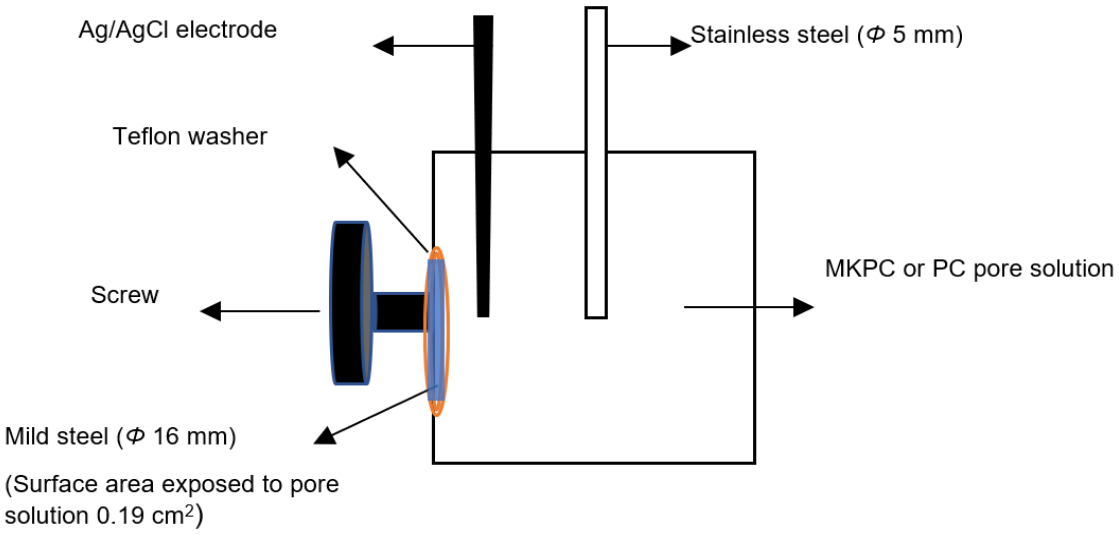

817

818 Fig. 3. Schematic diagram of the test setup for electrochemical measurements.

819

820

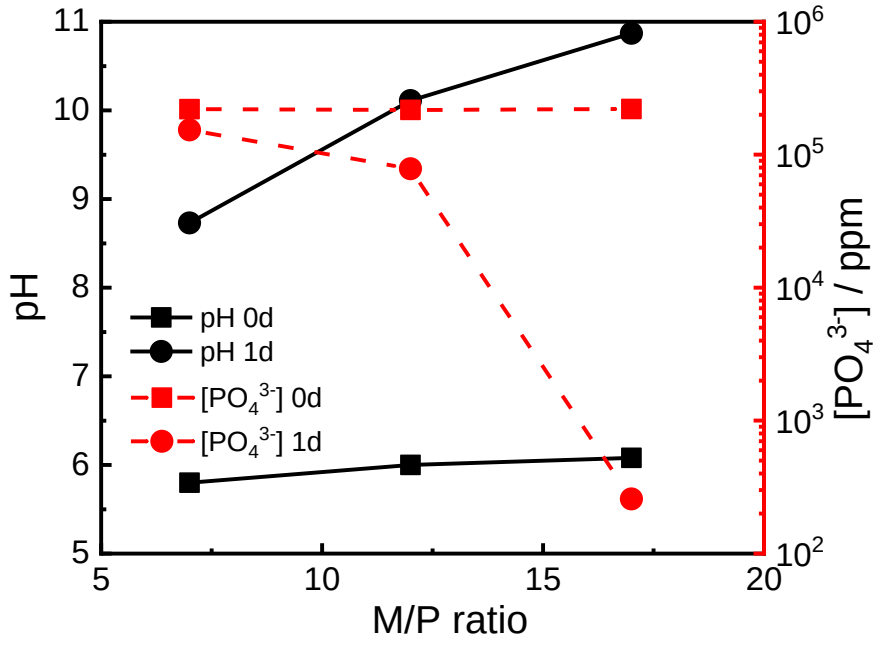

821

822 Fig. 4. pH level and PO_4^{3-} concentration of the extracted MKPC solutions.

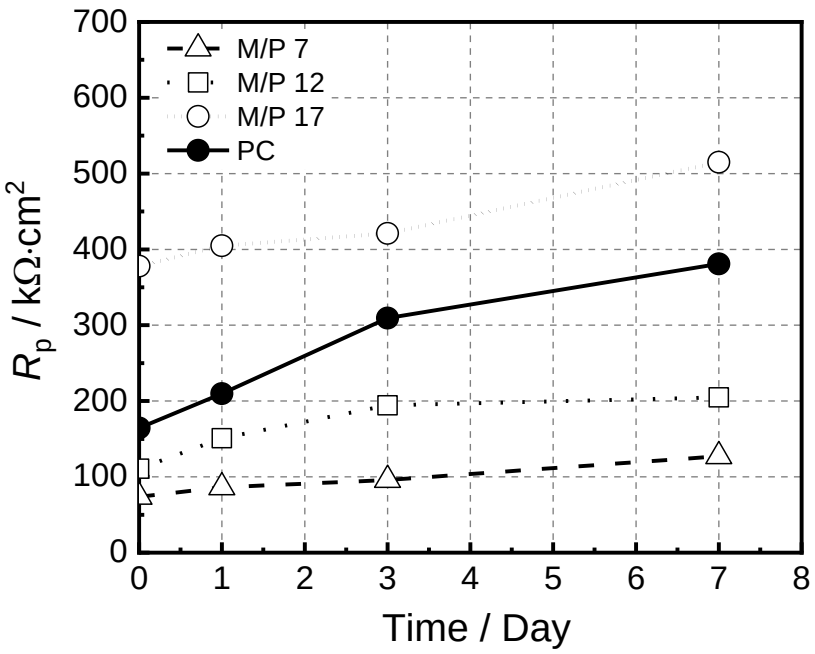

823

824 Fig. 5. LPR results of mild steel in MKPC and PC pore solutions.

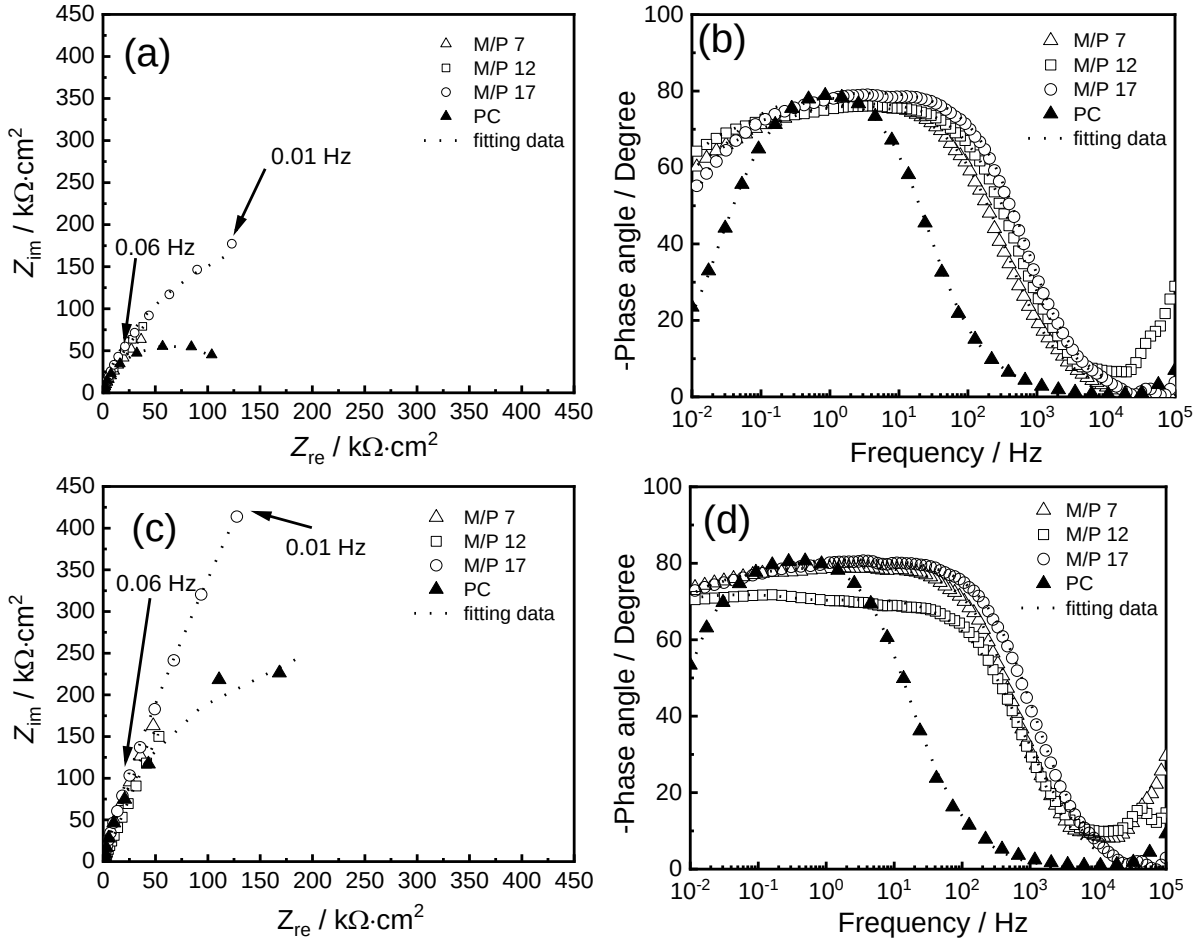

825 Fig. 6. EIS results for steel rebar immersed in MKPC and PC pore solutions: a)
826 Nyquist plot at 0 day; b) Bode phase plot at 0 day; c) Nyquist plot at 7 days;
827 d) Bode phase plot at 7 days.

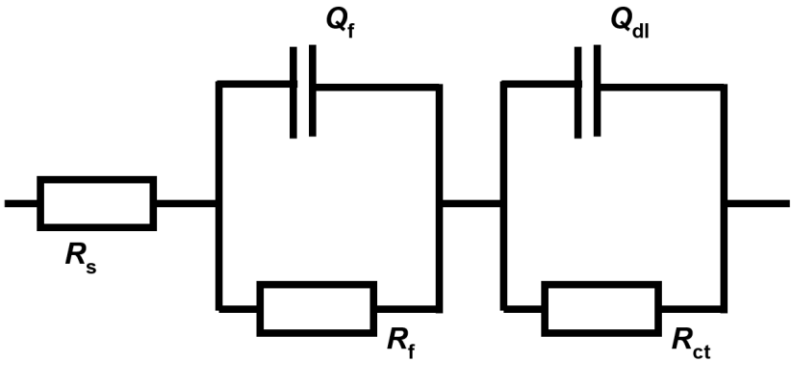

828

829 Fig. 7. Equivalent circuit for modelling EIS results.

830

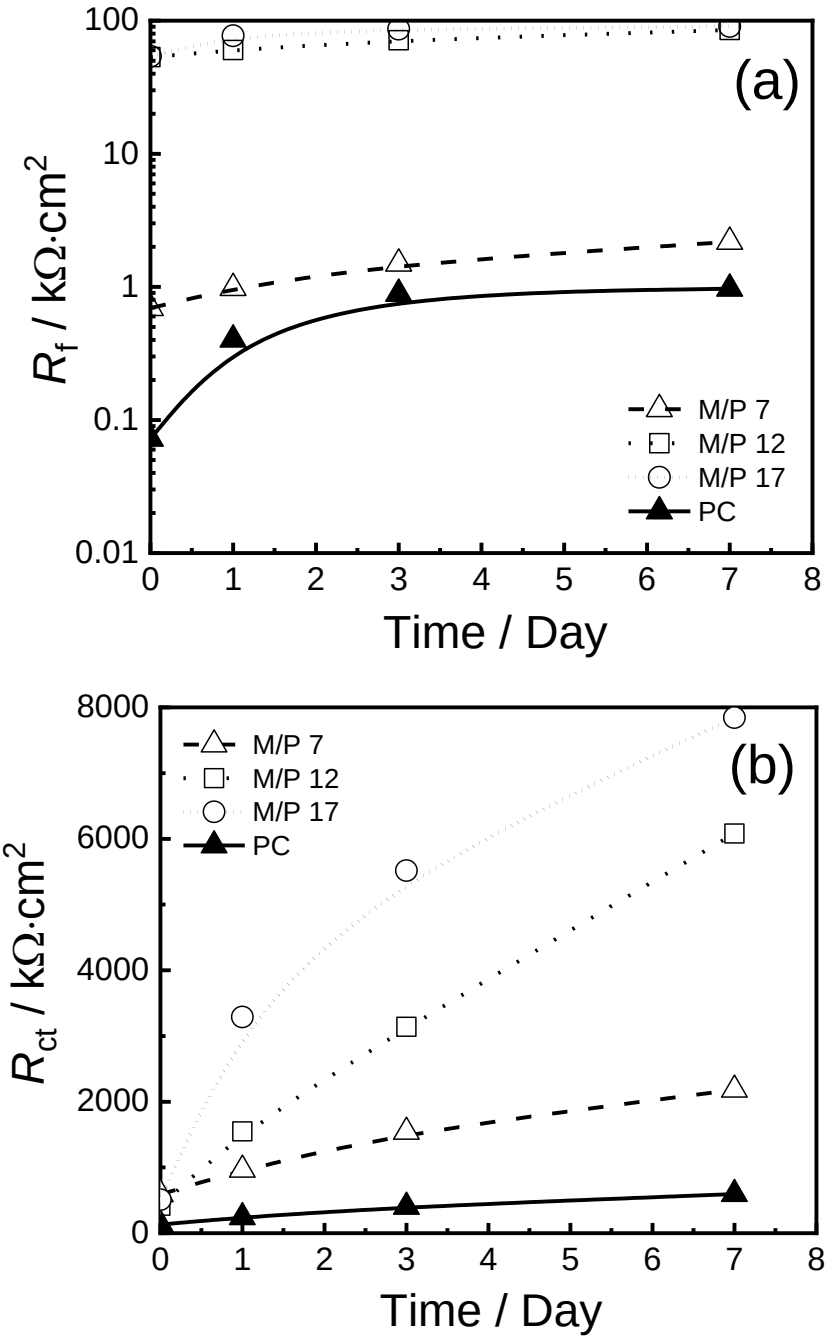

831

832

833 Fig. 8. The EIS fitting data in MKPC and PC pore solutions: a) R_f and b) R_{ct} with

834 curing time.

835

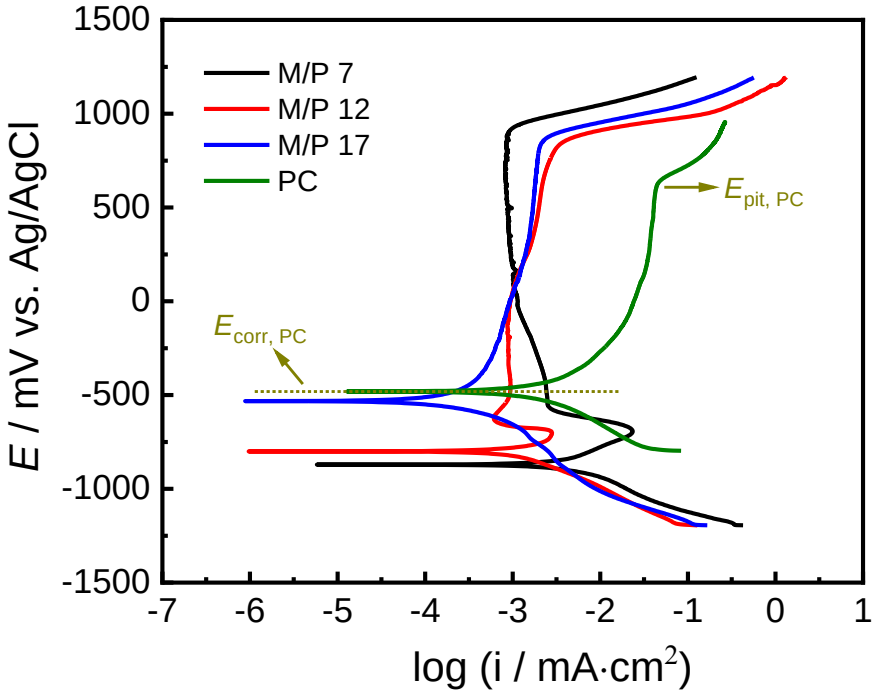

836

837 Fig. 9. Potentiodynamic polarization curves of mild steel at 3 days in MKPC and PC

838 pore solutions obtained at a scan rate of 0.16 mV s^{-1} (Note: the E_{corr} and E_{pit} of PC

839 specimen are illustrated as an example. The values for other specimens are not

840 shown).

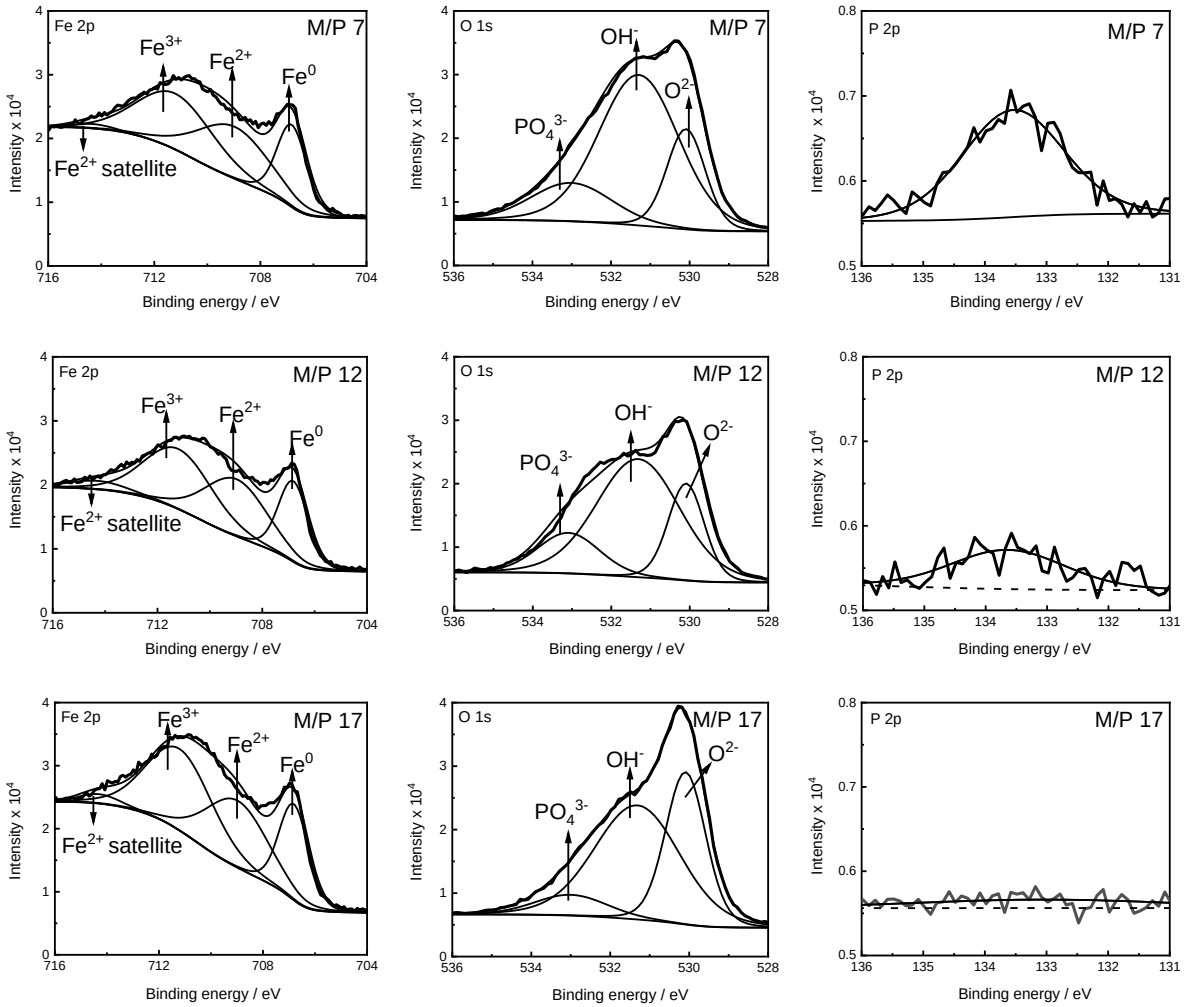

841 Fig. 10. The XPS spectra of mild steel in MKPC pore solutions.

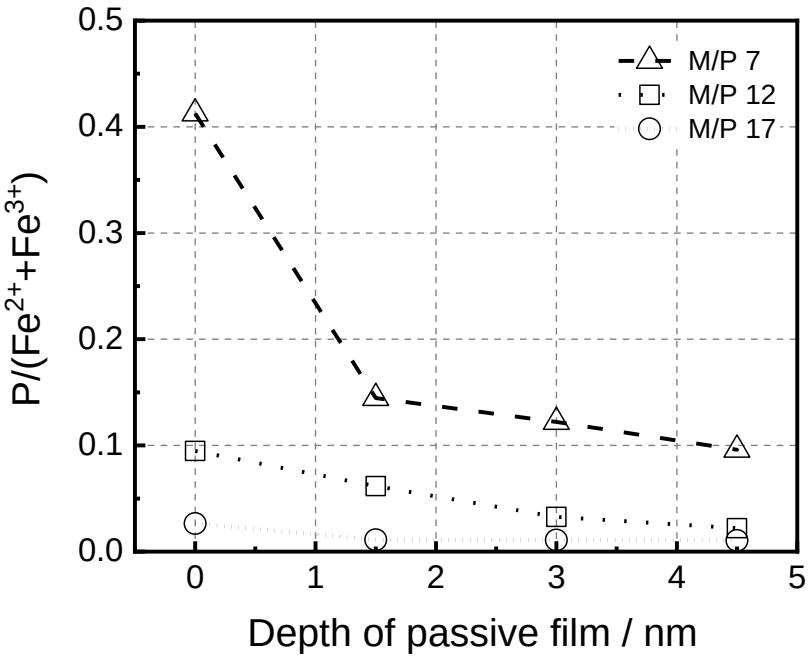

842

843 Fig. 11. The variation in the P/Fe ratio detected after 3 h immersion in MKPC pore

844 solutions.

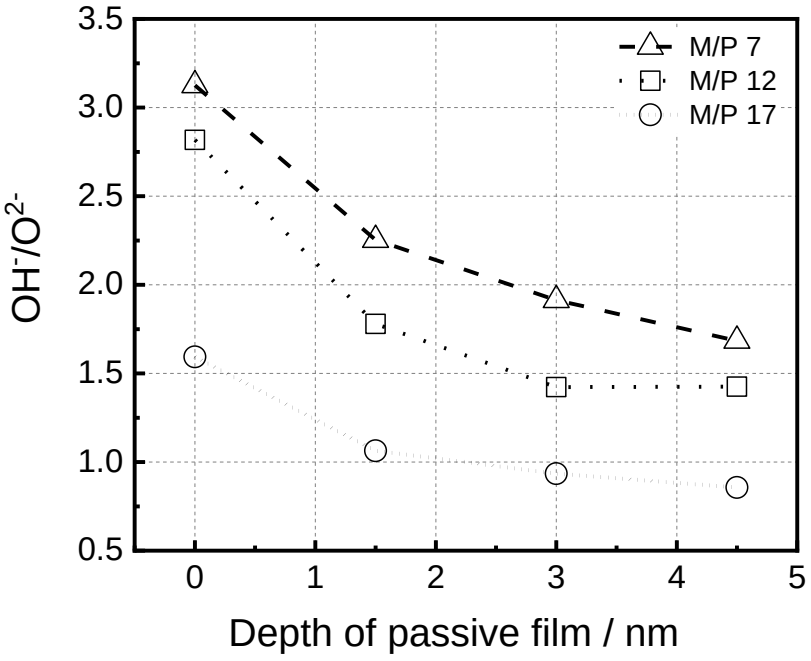

845

846 Fig. 12. The variation in the OH^-/O^{2-} ratio detected after 3 h immersion in MKPC pore

847 solutions.

848

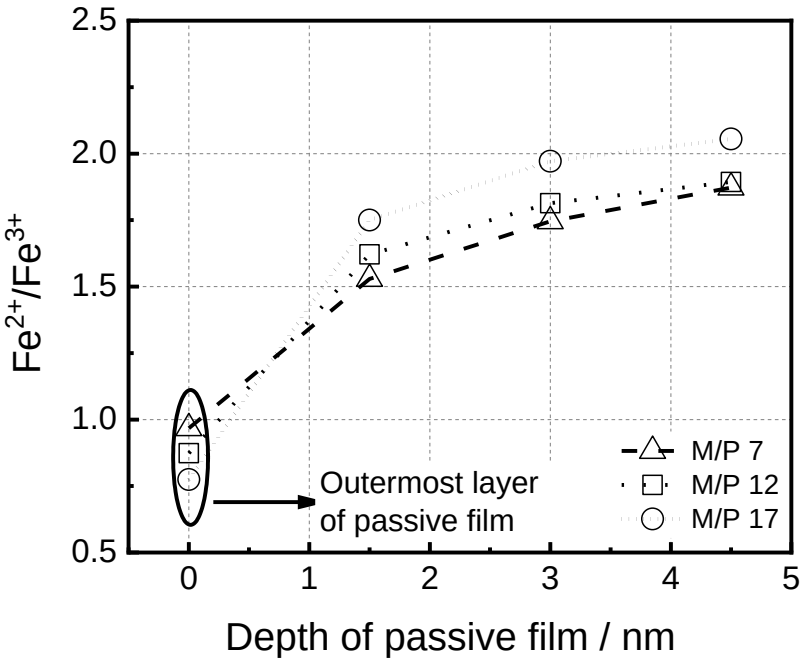

Fig. 13. The variation in the Fe^{2+}/Fe^{3+} ratio detected after 3 h immersion in MKPC pore solutions.

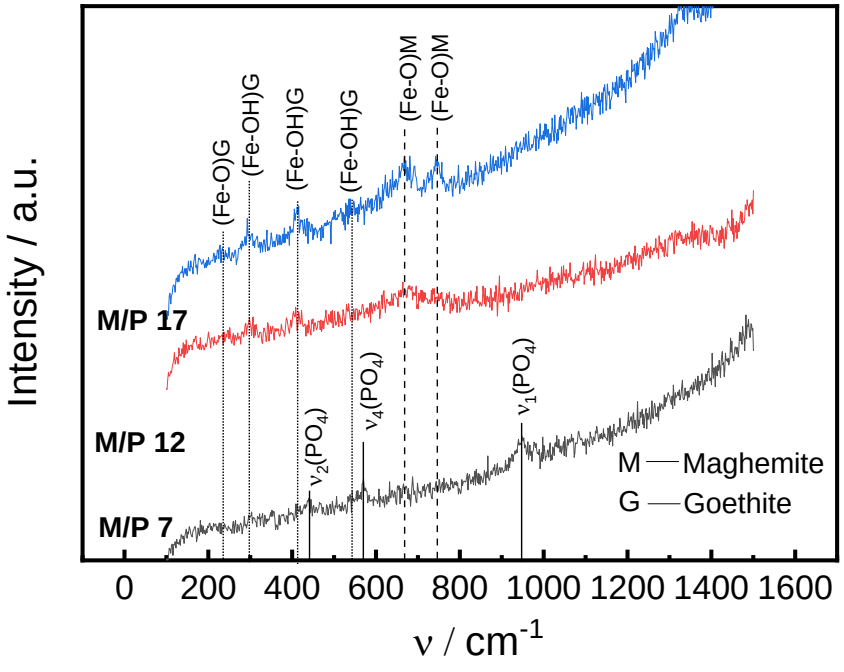

Fig. 14. Raman spectra of the steel surface immersed in MKPC pore solutions for 3 hours.

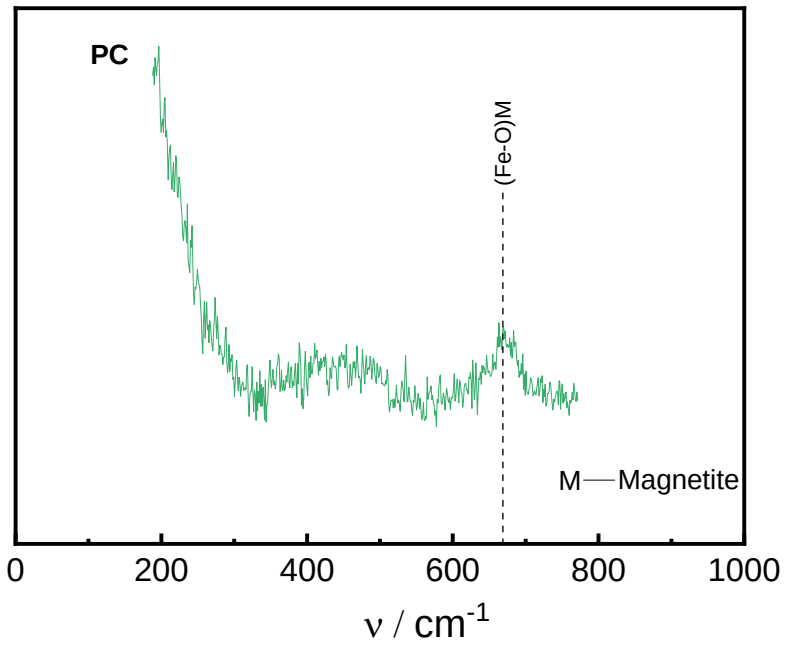

856

857 Fig. 15. Raman spectra of the steel surface immersed in PC pore solution.

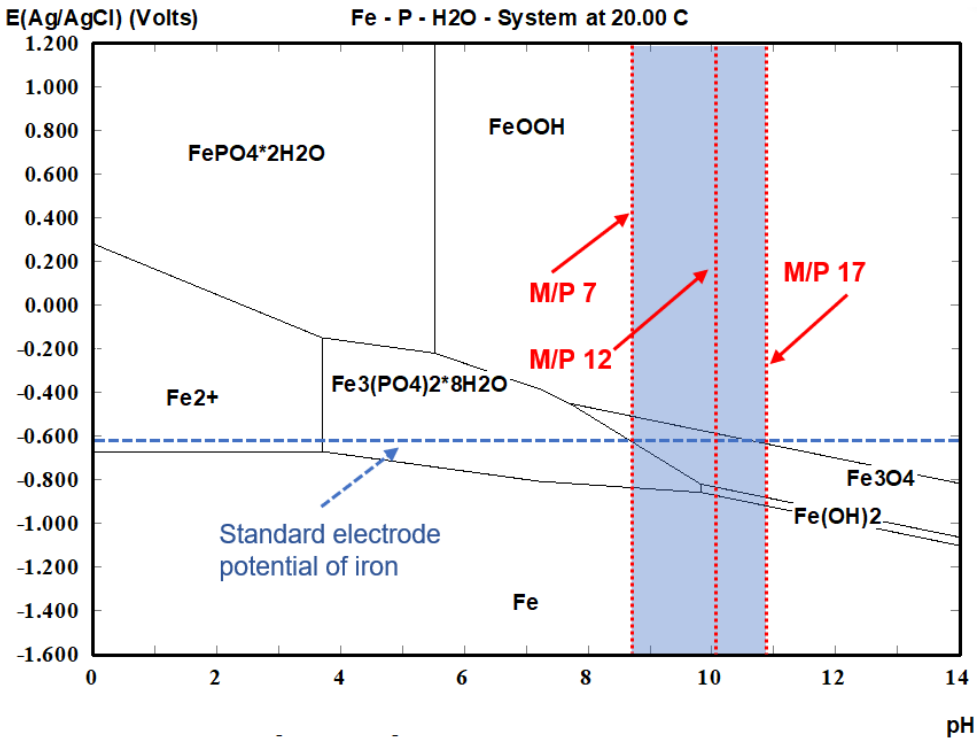

858

859 Fig. 16. Potential-pH diagram for the Fe-P-H_2O system at 20 °C.

860

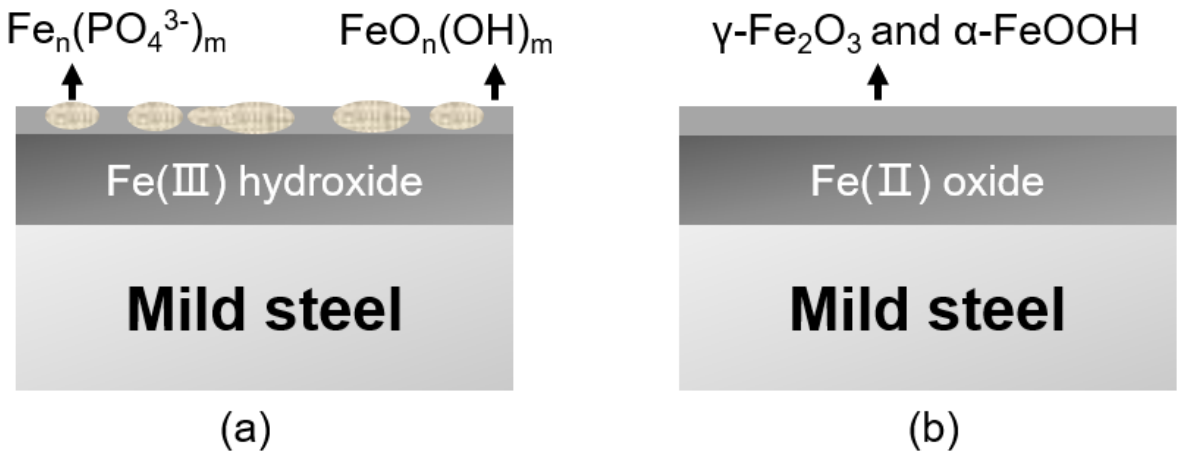

861

862 Fig. 17. Proposed passivation mechanism of mild steel in the MKPC pore solutions
863 of a) below pH 8.8 (pH 8.7 for M/P 7) and b) above pH 8.8 (pH 10.1 for M/P
864 12 and pH 10.9 for M/P 17).